



ISSN: 2321-2152

IJMECE

*International Journal of modern
electronics and communication engineering*

E-Mail

editor.ijmece@gmail.com

editor@ijmece.com

www.ijmece.com

An Observability Measurement for Range-Based Subsea Vehicle Localization

PT Balakrishna, AVN Deepthi, B Swapnika

Abstract:

In this work, we explore the associated observability problems with the overarching goal of localizing single and many AUVs utilizing range measurements. Global Navigation Satellite Systems and other geolocation systems are rendered ineffective underwater due to the absorption of electromagnetic radiation. Due to the high levels of error introduced by sensor bias and drift, AUV localization using dead reckoning techniques or cheap motion sensor units is not feasible. Trilateration algorithms are often used in localization systems to determine the distance between an AUV and a fixed network of transponders. Acoustic sensors play a key role in this process. These methods are costly and time-consuming to calibrate, and they can only detect AUVs within the region specified by the geometry of the transponders. An effective alternative to using mere transponder distance alone has been developed in recent years for use with AUVs. In this method, the onboard motion sensors of the AUV measure a variety of parameters, including depth, speed, and acceleration. Incorporating sound sensors into the system to allow AUVs to gauge their distance from one another is one potential next step for this concept. Given these developments, this study shows how the same mathematical model may manage relative and absolute vehicle localization. To further investigate how various forms of motion impact AUV localization performance, it adjusts observability ideas originally developed for nonlinear systems. We show that our proposed observability measure may improve the performance of an Extended Kalman filter by modeling this effect and testing it using a real-world marine vehicle. A modification will be made to the status of the filter observer as you drive.

Key words : We find terms like "observability metric," "submersible," and "range-only localization" among them.

Introduction

Autonomous underwater vehicles (AUVs) have gained popularity in the last several decades and are currently used extensively across many sectors, including as the military, academia, and the tourist sector. Helping marine scientists with their oceanographic environmental monitoring efforts is only one of many potential applications for autonomous underwater vehicles (AUVs). For AUVs to complete their missions autonomously, precision locating skills are critical. While GNSSs and similar localization systems are known to work effectively above water, their

utility is severely restricted when the vehicles are submerged since electromagnetic radiation is attenuated when employed underwater. To precisely determine an AUV's position, dead reckoning integrates inertial and velocity data. Nevertheless, number-wise, because of the Because dead reckoning accounts for sensor bias, drift, noise, and noise, it is only practical for shallow dives. But it may be swayed by outside forces and faulty models. Frequent surface visits may be necessary for the AUV to maintain an up-to-date

Associate Professor¹, Assistant Professor^{2,3}
(Department of Electronics and Communication Engineering)
priyadarshini institute of technology

GNSS position. Another common method for underwater localization is to use auditory equipment to determine the relative bearing and height of locations, as well as the distances between them. Complex jobs have made extensive use of commercially available solutions such as Ultra-Short Baseline, Long Baseline, and Short Baseline systems. Long Baseline (LBL) systems use regularly spaced transponders dropped to a certain depth for acoustic localization. The autonomous underwater vehicle (AUV) uses the time it takes for the reflected sound waves to return to its receiver after requesting the transponders to find the distance. The trilateration approach is then used to find the AUV's position. In Short Baseline (SBL) systems, the transducers are placed on top of a surface vessel and are separated by several meters. By interacting with a transponder attached to the submerged AUV, the surface component is responsible for triangulating its position. A compact, self-contained device put aboard a support vessel measures the relative phases of the signals given by the surface segment and stores the findings. This device is used to estimate the locations of an AUV. The third option includes communicating the predicted position of the AUV. A new approach to AUV localization has evolved, using a single transponder (beacon) and transducer, with the goal of streamlining processes without increasing sensor costs. The AUV may utilize this technique to find itself instead of depending on data from a central transmitter. A depth sensor, Doppler log, and inertial measurement unit are just a few of the many auxiliary sensors used by the AUV. Recent publications [1-4] demonstrate that this localization problem—which goes by many names, such as range-only localization and single beacon localization—is getting a lot of attention. This study introduces an observability metric for the single beacon localization problem by using the local weak observability properties of a chosen non-linear system. Therefore, in order to make sure everything is clear and comprehensive, we provide a brief summary of important prior work in the subject that addresses the problems mentioned.

Modelling the Observability of Systems

First, we take a look at the problem of relative localization between two AUVs. The North East Down (NED) convention specifies an inertial, earth-fixed reference frame I , and a frame v,i with an origin fixed at the centroid of the i -th vehicle ($i = 1, 2$) and in parallel to I (see Figure 1). From here on, we shall say that $v_{v,1} = dx_{v,1}/dt$ and $v_{v,2} = dx_{v,2}/dt$, where IR^3 is the coordinate system of vehicle 1 and $x_{v,2}$ is the coordinate system of vehicle 2, and that inertial velocities $v_{v,1}$ and $v_{v,2}$ are equal. Here, $x = x_{v,2}x_{v,1}$ represents the system state and $v = v_{v,2}v_{v,1}$ represents the relative velocities of the vehicles. Our working assumption is that inertial sensors can measure not only the distance between cars but also their velocities and depths relative to one another. The first-order kinematic model of the vehicles' relative motion is represented by the following notation: x is the current state, v is the input, and $y \in IR^2$ is the observable output vector. It is a function, h_1 , of the two vehicles' distance from each other in geometric units ($kaki$) and the depth difference (x_3).

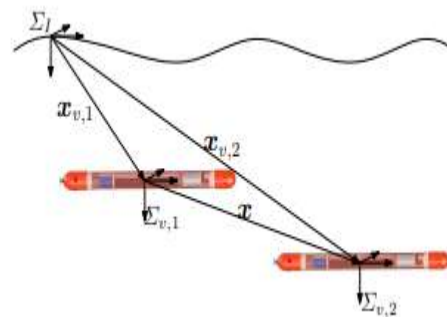


Figure 1. Reference systems: Σ_I is the inertial, earth-fixed frame and $\Sigma_{v,i}$ are the moving frame with the origin fixed in the i -th vehicle ($i = 1, 2$).

In the literature, the range-based localization problem is usually studied in 2D. Here, we start by explicitly including a third dimension (depth) to fully capture manoeuvres that include diving. Once we have shown that the vertical component does not affect the observability of the system, we then move on to the 2D case. Notice also that, since the above model is defined in terms of relative motions, it captures the kinematics of both single beacons, as well as relative multi-

vehicle localization problems. To discuss the observability properties of the system in Equation (1), we first recall some basic observability concepts for non-linear systems, summarize important local weak observability properties and describe an observability rank condition; we then apply the latter condition to our specific case.

Single Beacon Localization:

Numerical Simulations This section presents the results of numerical simulations that illustrate the effectiveness of the observability index proposed in assessing the performance that can be obtained with a single beacon localization algorithm. Specifically, we consider a single-beacon localization algorithm that is obtained by implementing an Extended Kalman Filter for a discrete-time version of Equation (5), and we evaluate its performance under different operational conditions (e.g., different vehicle speeds and trajectories) in light of the proposed metric. The system state equation is assumed as:

$$\begin{cases} \mathbf{x}_{k+1} = \mathbf{x}_k + T\mathbf{v}_k + \mathbf{w}_k \\ y_{k+1} = \frac{1}{2}\mathbf{x}_k^T \mathbf{x}_k + \mu_k \end{cases}$$

where \mathbf{w}_k and μ_k are process and measurement noises, assumed as zero-mean Gaussian noise with

$$\mathbf{w}_k \sim \mathcal{N}(0, \mathbf{R}_w) \text{ and } \mu_k \sim \mathcal{N}(0, R_\mu); T$$

is the sample time. An EKF filter for Equation (16) was implemented using the following standard equations: (1) Time update of state and estimation error covariance:

$$\begin{aligned} \hat{\mathbf{x}}_{k+1}^- &= \hat{\mathbf{x}}_k^+ + T\mathbf{v}_k \\ \mathbf{P}_{k+1}^- &= \mathbf{P}_k^+ + \mathbf{R}_w \end{aligned}$$

(2) Measurement updates of state and estimation error covariance:

$$\begin{aligned} \mathbf{K}_{k+1} &= \mathbf{P}_{k+1}^- \mathbf{H}_k^T [\mathbf{H}_k \mathbf{P}_{k+1}^- \mathbf{H}_k^T + R_\mu]^{-1} \\ \hat{\mathbf{x}}_{k+1}^+ &= \hat{\mathbf{x}}_{k+1}^- + \mathbf{K}_{k+1} (y_k - \frac{1}{2}\mathbf{x}_{k+1}^-^T \mathbf{x}_{k+1}^-) \\ \mathbf{P}_{k+1}^+ &= (\mathbf{I} - \mathbf{K}_{k+1} \mathbf{H}_k) \mathbf{P}_{k+1}^- \end{aligned}$$

here \mathbf{H}_k is the linearization of the output measurement equation computed for $\mathbf{x} = \hat{\mathbf{x}} - \mathbf{k}+1$, i.e., $\mathbf{H}_k = \hat{\mathbf{x}}^T - T \mathbf{k}+1$. The covariance matrix of the process and measurement noises are assumed to be $\mathbf{R}_w = \text{diag}([0.1 \ 0.1])$ (where $\text{diag}([a_1 \dots a_n])$ is a diagonal matrix whose diagonal entries starting in the upper left corner are a_1, \dots, a_n) and $R_\mu = 5$, respectively, while the EKF covariance matrix is initialized as $\mathbf{P} + 0 = \text{diag}([2 \ 2])$. In the first simulated scenario, the vehicle was commanded to execute a lawn-mowing maneuver (consisting of a succession of orthogonal line segments). The speed of the vehicle was kept constant and equal to 1 m/s along each segment, except when required to change orientation during the transition from one to the next segment; in the latter case, the vehicle was supposed to have the capability to rotate in place. Figure 5 shows the path followed by the vehicle and its position as estimated using the EKF; the figure also shows the ellipsoid corresponding to the EKF covariance matrix along the path.

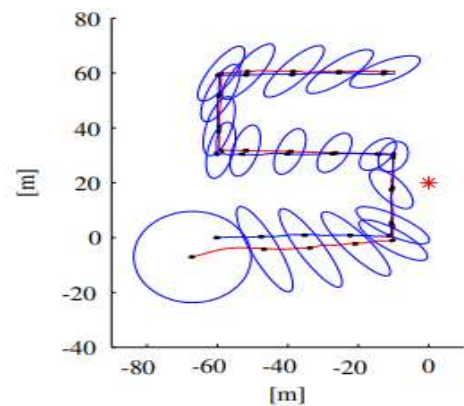


Figure 2. Real (blue) and estimated (red) path of a vehicle moving along orthogonal segments of a line using an Extended Kalman Filter (EKF) and range measurements from a single beacon in position [0, 20] m. The ellipses represent the covariance matrix of the EKF, while the red star represents the position of the transponder.

Figure 2 shows the time-evolution of different variables of interest: the norm of the estimation error, the distance of the vehicle from the transponder, the eigenvalues of the EKF covariance matrix and the observability index, $C - 1$. Notice that the lower eigenvalue of the EKF covariance matrix quickly

decreases to a value related to the range measurement covariance; the higher eigenvalue, however exhibits more complicated dynamics related to the AUV path and decreases when the observability index takes large values. The intervals where the observability index, C^{-1} , is equal to zero correspond to the rotation of the AUV in place, when it moves from one segment to the following.

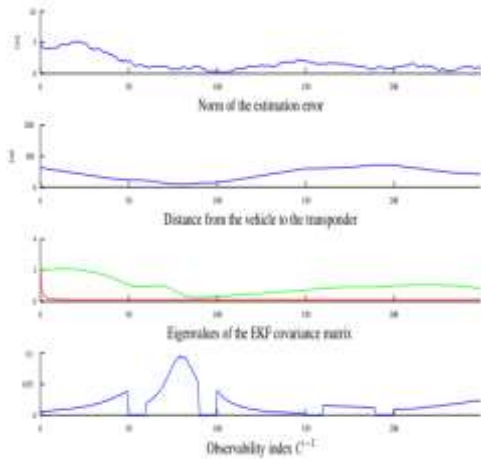


Figure 3. Variables of interest related to the paths in Figure 5: observability index C^{-1} , eigenvalues of the EKF covariance matrix, distance from the vehicle to the transponder and the norm of the estimation error.

We performed two sets of simulations with the vehicle driving around circumferences centered on the transponder to further illustrate the connection between the observability index and the filter's performance. The first round of simulations included driving the vehicle at varying speeds (0.5 m/s, 1 m/s, 1.5 m/s, and 2 m/s), which correspond to different values of the observability index (see Figure 7 for the pathways). Similar remarks apply to the higher eigenvalues of the EKF covariance matrix, as shown in Figure 8, indicating that the estimate error reduces more slowly along the route with a lower instantaneous observability index (solid line, conducted at the lowest speed).

In-Vehicle Tests

Experiments Here we report the outcomes of our attempts to put the observability index presented in this work to the test in a realistic

setting. Beacon detection, which may be thought of as the inverse issue of single beacon localization discussed above, is the topic of this article. In this case, the vehicle already knows its location and must estimate the beacon's position using range measurements. The field experiments were conducted using an autonomous marine vehicle fitted with an acoustic range device that could determine its distance from an acoustic transponder anchored to the bottom at a known place. The trials were conducted in Lisbon, Portugal, in the Nations Park (the former location of Expo 98) (Lat: 38.766, Long: 9.03).

Construct for Experiment

The experiments were conducted using an ASV rather than a real AUV due to practical considerations. Because of this, the beacon detecting system could be tested rapidly without having to wait for the AUV localization tests. Actually, with the right setup, a GNSS system may be used to ascertain the ASV's whereabouts. Still, when looking at it through the lens of practical acoustics, the challenge of AUV-based single beacon localization and the difficulties of ASV-based beacon recognition based on range measurements alone are similar. Laboratory of Robotics and Systems in Engineering and Science (LARSyS; see Figure 11) at the Instituto Superior Técnico of Lisbon designed Medusa, the ASV used in the experiments. The vehicle's agility is enhanced by its two side thrusters, which may be controlled independently for surge and yaw. Connectivity options include WiFi for land-based devices and an acoustic modem/ranging unit (Tritech Micron Modem; see Figure 12 (right)) for underwater communication. The vehicle also incorporates a Global Navigation Satellite System (GNSS) and an Attitude and Heading Reference System (AHRS). Submerged at a known location at a depth of 2 meters, the transponder is only a Tritech Modem unit (Figure 12 (left)) set up to respond to queries sent by the surface modem. In turn, the latter figures out how far apart the surface and underwater units are by multiplying the time it takes for a signal to go from one location to another by the water's specific speed. In order

to charge and test the transponder, it was



attached to surface support system via wire.

Figure 5. The Medusa autonomous surface vessel.



Figure 6. Fixed transponder (left) and acoustic modem/ranging device on the Medusa nose cone (right).

The distance between the ASV and the transponder relies on the speed of sound in water, thus every effort was taken to measure it accurately using a specialized equipment every day before the experiments started. The ASV was given two sets of instructions for the observability study: one set of circular pathways centered on the transponder, and another set of parallel/orthogonal segments, some of which were radial with regard to the transponder. The ASV meticulously captured and stored all of its GNSS coordinates, compass directions, and range measurements. The processed data was run through an Extended Kalman Filter to determine its effectiveness, using equations that are identical to Equations (17)-(19). The filter was designed for on-board ASV implementation, therefore it compensates for transient range measurement errors and, in the absence of range data (a sample is acquired every few seconds), notifies the observer based only on velocity (as in a traditional dead reckoning approach). Based on the examples from numerical simulations, we assume that the process and measurement noises have covariance matrices $R_w = \text{diag}([0.1 \ 0.1])$ and $R = 5$, respectively. In contrast, the EKF covariance matrix is initially set as $P + 0 = \text{diag}([2 \ 2])$. Just to review, the theoretical and practical challenges of estimating the autonomous vehicle's location relative to the transponder are identical to those of predicting the transponder's position (as if it were unknown) given the vehicle's known position. The tests described below pertain to the second scenario. Experimental Findings Consistent results were obtained after many experiments were carried out and their data were examined. To begin, we measured a 100 by 100 meter square and guided the ASV in a series of parallel and orthogonal lines. In Figure 13, you can see the ASV's flight path. In the backdrop, you can make out the distant base station (Medusa Base) that takes data from the ASV and stores it. The black squares show the estimated location of the transponder at

different points in the mission.

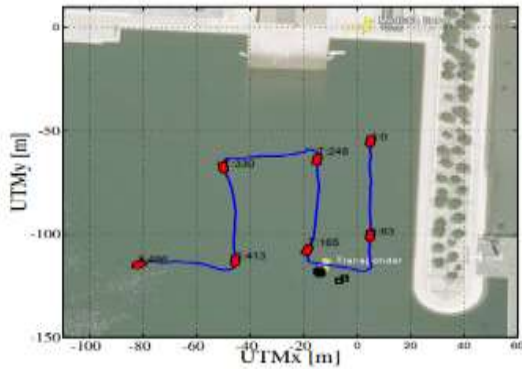


Figure 7. Path followed by the Medusa Autonomous Surface Vessel (ASV) during the first mission.

It is possible to find data relevant to the observability analysis in Figure 7. With actual relative displacement included, the top graph shows the computed inverse of the condition number of the observability matrix in Equation (9). By combining the precise position of the transponder with the ASV's GNSS data, we can determine the actual displacement, x , that has occurred between the two. The second plot in Figure 14 shows the observer's estimation inaccuracy. Within a circle centered on the ASV and having a radius equal to the range measurement, the filter is configured to estimate the transponder's position to be 10 meters away from its real location. The distance between the ASV and the transponder is shown in Figure 14, third figure, by comparing the blue data from the acoustic ranging device with the red readings from the GNSS. Keep in mind that although the modem reading is quite accurate, updates take a long time and there are sometimes brief periods when there is no connection (which is expected, considering the challenging conditions of sound transmission in very shallow waters). The values of are shown in the fourth panels of Figure 14 (with Equation (12) as a reference), while the upper and lower eigenvalues of the EKF covariance matrix are shown in the final graphs. Important aspects of the mission that must be emphasized at this time are shown in Figures 13 and 14. Within the 80-180 s window when the ASV approaches the transponder, the filter error decreases at a faster rate than when it recedes from it. Also, remember that the noise covariance in process measurements raises

both EKF eigenvalues, yet dead-reckoning data keeps the filter error low when range measurements aren't available. The second experiment, seen in Figure 15, included having the ASV circle the transponder. Figure 16 shows that the ASV keeps a steady and a speed that is almost the same. The observability index, for example, reaches its maximum value at 2. Unlike the prior mission, this one exhibits a gradual and quick decrease in the filter estimation error, and the larger eigenvalue of the EKF covariance matrix remains contained over the whole experiment.

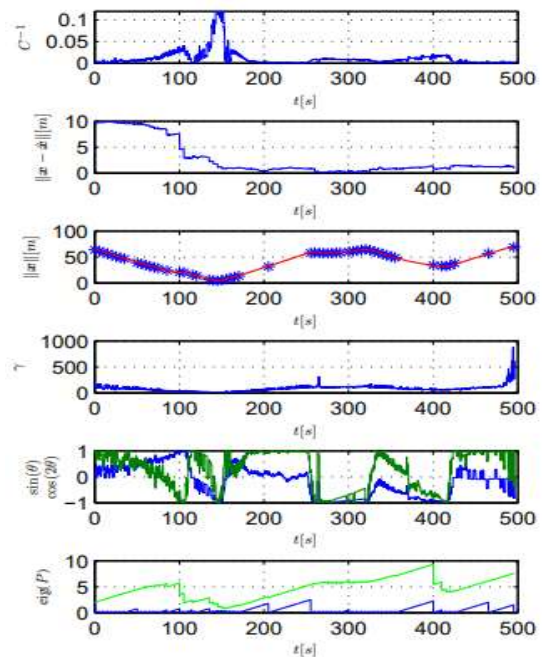


Figure 8. Observability parameters during the first mission: inverse of condition number (top plot), norm of estimation error (second plot from top), measurements of the range between the vehicle and the transponder (blue stars) and GNSS (red line) (third plot), γ (fourth plot), $\sin(\theta)$ (blue) and $\cos(2\theta)$ (green) (fifth plot) and eigenvalues of the EKF covariance matrix (last plot).

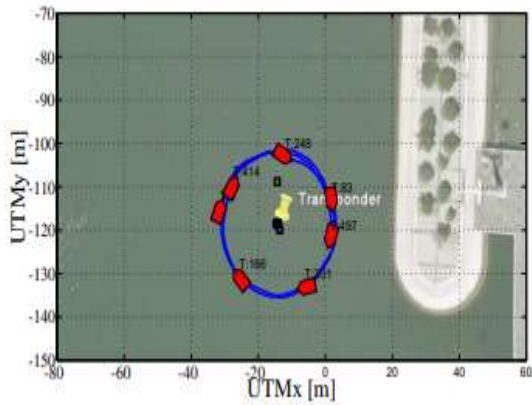


Figure 9. Path of the robot during the second mission.

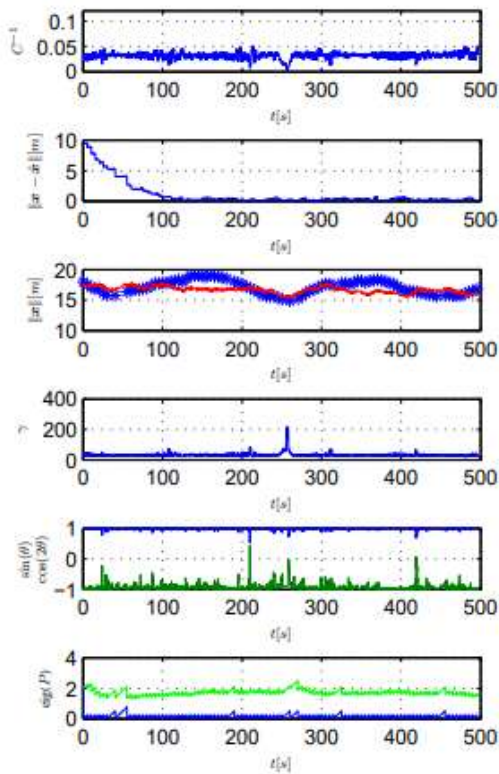


Figure 10. Observability parameters during the second mission: inverse of condition number (top plot), norm of estimation error (second plot from top), measurements of the range between the vehicle and the transponder (blue stars) and GNSS (red line) (third plot), γ (fourth plot), $\sin(\theta)$ (blue) and $\cos(2\theta)$ (green) (fifth plot) and eigenvalues of the EKF covariance matrix (last plot).

Finally, the ASV was programmed to travel along a sinusoidal path (shown in Figures 17 and 18), an example in which the observability index has a significant impact on the speed

with which the estimation error decreases and the bounds within which the EKF covariance eigenvalues matrix can be calculated. In the experiment's final phase, range measurements are received in a dispersed fashion, and the increase in EKF eigenvalues due to the AUV process noise covariance can be observed. The attached multimedia file depicts a reconstruction, using experimental data, of the observability metric analysis in relation to the previously provided case studies. Animations showing ASV movement, EKF filter effectiveness, and observability index variability across many case studies are shown in the film.

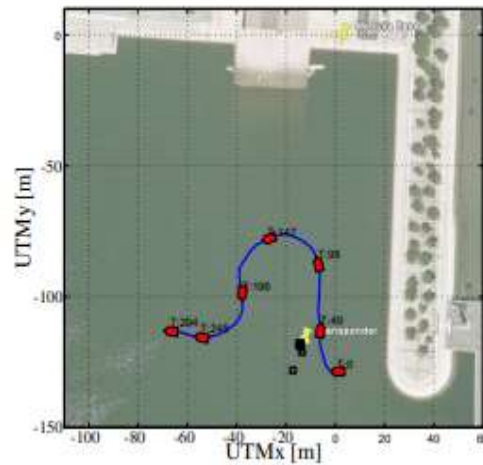


Figure 11. Path of the robot during the third mission.

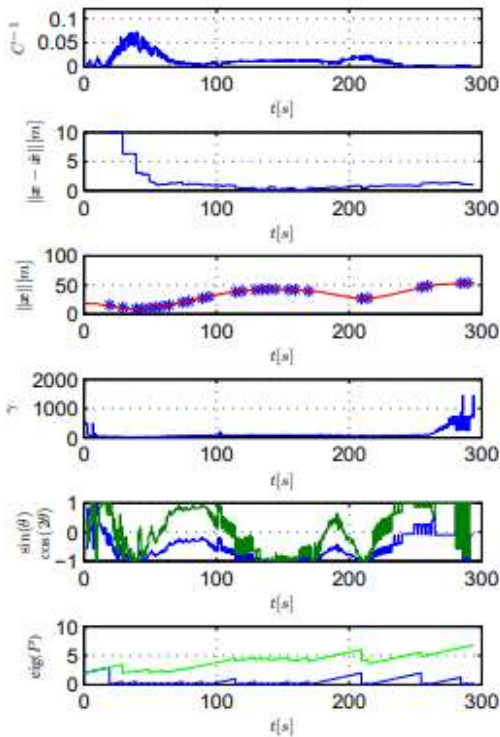


Figure 12. Observability parameters during the third mission: inverse of condition number (top plot), norm of estimation error (second plot from top), measurements of the range between the vehicle and the transponder (blue stars) and GNSS (red line) (third plot), γ (fourth plot), $\sin(\theta)$ (blue) and $\cos(2\theta)$ (green) (fifth plot) and eigenvalues of the EKF covariance matrix (last plot)

Conclusion

Here we analyzed two separate localization issues, one involving the structural observability of a single beacon and the other involving the relative position of two AUVs estimated from range data alone. A proposed measure based on nonlinear observability theories was used to quantify the observability of vehicle motions. Analyses of simulations and experimental verification demonstrated the success of the proposed measure. In the future, researchers will concentrate on studying different types of observers and developing the best real-time trajectory planning algorithms that employ the recognized metric. We will also go over how to apply these ideas to a situation with more than one car.

References

- [1]. *Underwater Vehicles' Synthetic Long Baseline Navigation* (Larsen, M.). Pages 2043–2050 from the *Oceans 2000 MTS/IEEE Conference*, held in Providence, Rhode Island, USA, from September 11th to the 14th, 2000.
- [2]. *Underwater navigation in the presence of unknown currents using range measurements from a single location is the subject of Gadre and Stilwell's work.* Articles 565–661 from the *2005 American Control Conference*, held in Portland, USA, from June 8th to the 10th, 2005.
- [3]. *Automatic underwater vehicle cooperative localization* by Bahr, Leonard, and Fallon. The volume 28, pages 714-728, of the *2009 International Journal of Robotics Research*, was published.

In their paper "Preliminary Deep Water Results in Single-Beacon One-Way-Travel-Time Acoustic Navigation for Underwater Vehicles," Webster, Singh, Eustice, and Whitcomb [4] present their findings. From October 10-15, 2009, in St. Louis, MO, USA, this paper was presented at the 2009 IEEE/RSJ International Conference on Intelligent Robots and Systems. Its pages range from 2053 to 2060.

The STRONG algorithm, developed by Hartsfield and used to REMUS autonomous underwater vehicles, is a single transponder range-only navigation scheme [5]. Doctoral dissertation submitted in August 2005 to the Woods Hole Oceanographic Institution and the Massachusetts Institute of Technology in Cambridge, Massachusetts, USA.

- [6]. *Gadre, A. Analysis of Observability in Underwater Vehicle Navigation Systems. Doctoral dissertation, Blacksburg, Virginia, USA, 2007 from Virginia Polytechnic Institute and State University.*

Notes on the Observability of Single Beacon Underwater Navigation [7]. Ross, A.;

Jouffroy, J. Durham, New Hampshire, USA, August 2005: *Proceedings of the International Symposium on Unmanned Untethered Submersible Technology*.

Underwater Navigation with a Single Transponder: An Algebraic Viewpoint by Jouffroy and Reger [8]. Volume 1789–1794 of the Proceedings of the 2006 IEEE International Conference on Control Applications, Symposium on Computer-Aided Control Systems Design, and International Symposium on Intelligent Control, held in Munich, Germany from October 4th to the 6th, 2006.

Using Collaborative Localization for Submersibles Without Human Intervention [9]. Bahr, A. In February 2008, I completed my doctoral studies at the Massachusetts Institute of Technology and the Woods Hole Oceanographic Institution in Cambridge, Massachusetts, USA.

In their paper "Cooperative AUV Navigation using a single maneuvering surface craft," Fallon, Papadopoulos, Leonard, and Patrikalakis [10] discuss the use of AUVs in a cooperative manner. Journal of Robotics Research 2010, 29, 1461–1474.

According to a study by Singh et al. (2011), "Underwater Acoustic Navigation with the WHOI Micro-Modem," the authors used the WHOI Micro-Modem. Includes pages 1-4 from the 2000 MTS/IEEE Oceans Conference and Exhibition, held in Providence, Rhode Island, USA, from September 18th to the 21st.

Cooperative Localization of Marine Vehicles Using Nonlinear State Estimation [12]. Papadopoulos, G., Fallon, M., Leonard, J., Patrikalakis, N. Pages 4874–4879 of the 2010 IEEE/RSJ International Conference on Intelligent Robots and Systems, held in Taipei, Taiwan, from October 18th to the 22nd, 2010.

[13] Observability measurements and their application to GPS/INS. IEEE Trans. Veh. Technol. 2008, 57, 97-106. Hong, S.; Chun, H.; Kwon, S.; Lee, M.

One-Beacon Acoustic Navigation for an AUV with Unknown Ocean Currents [14]. Sa'ude, J.; Aguiar, A. Volume 8, Issue 3, Pages 298–303, Eighth International Federation of Applied Control (IFAC) Conference on Manoeuvring and Control of Marine Craft, Guarujá (SP), Brazil, September 16–18, 2009.

Single-range assisted navigation and source localization: Observability and filter design [15]. Batista, P., Silvestre, C., Oliveira, P. Statistical Control Letters, 2011, 60, 665-673.

[16]. In Intell. Serv. Robot 2011, 4, 259-270, Casalino, G., Caiti, A., Turetta, A., and Simetti, E. presented RT2, which stands for real-time ray-tracing for underwater range assessment.

[17]. Relative Pose Observability Analysis for 3D Nonholonomic Vehicles Based on Range Measurements Only. Parlange, G.; Pedone, P.; Indiveri, G. This paper was presented at the 9th International Federation of Advisory Councils for the Control and Manoeuvring of Marine Craft (IFAC 2012) in Arenzano (GE), Italy, from September 19th to the 21st.

The generalized informational correlation is a measure of observability [18]. The authors are Chen, Hu, Li, and Sun. Pages 5570–5574 from the 2007 IEEE Conference on Decision and Control held in New Orleans, Louisiana, USA, 12–14 December.

C. Jauffret's work on nonlinear regression's observability and Fisher information matrices [19]. 2007, 43, 756-759, IEEE Transactions on Aerospace Electronic Systems.

To track bearings alone: a hybrid coordinate system method [20]. Grossman, W. Included in the proceedings of the 30th IEEE Decision and

Control Conference, held in December 1991 in Brighton, UK, pages 2032–2037.